PROCEEDINGS OF SCIENCE

ONLINE ICRC 2021
THE ASTROPARTICLE PHYSICS CONFERENCE
Berlin | Germany
37th International Cosmic Ray Conference
12–23 July 2021

Response functions of semi-leaded neutron monitor count rates and leader rates from latitude surveys during 2019-2020

P. Yakum,[a,*] S. Khamphakdee,[a] W. Nuntiyakul,[a] D. Ruffolo,[b] P. Evenson,[c] P.-S. Mangeard,[c] A. Sáiz,[b] C. Banglieng,[d] A. Seripienlert,[e] P. Jiang,[f] P. Chuanraksasat,[e] K. Munakata,[g] J. Madsen,[h] B. Soonthornthum[e] and S. Komonjinda[a]

[a] *Department of Physics and Materials Science, Faculty of Science, Chiang Mai University, Chiang Mai 50200, Thailand*

[b] *Department of Physics, Faculty of Science, Mahidol University, Bangkok 10400, Thailand*

[c] *Department of Physics and Astronomy, University of Delaware, Newark, DE 19716, USA*

[d] *Department of Physics, Faculty of Science and Technology, Rajamangala University of Technology Thanyaburi, Pathum Thani 12110, Thailand*

[e] *National Astronomical Research Institute of Thailand (NARIT), Chiang Mai 50180, Thailand*

[f] *Polar Research Institute of China, Pudong, Shanghai 200136, China*

[g] *Physics Department, Shinshu University, Matsumoto, Nagano 390-8621, Japan*

[h] *Wisconsin IceCube Particle Astrophysics Center, University of Wisconsin-Madison, WI 53703, USA*

E-mail: panutda_y@cmu.ac.th, sidarat_k@cmu.ac.th, waraporn.n@cmu.ac.th, david.ruf@mahidol.ac.th, evenson@udel.edu, psmangeard@gmail.com, alejandro.sai@mahidol.ac.th, bchanoknan@gmail.com, achara@narit.or.th, jiangpeng@pric.org.cn, pongpichit.ch@gmail.com, kmuna00@shinshu-u.ac.jp, jim.madsen@icecube.wisc.edu, boonrucksar@narit.or.th, siramas.k@cmu.ac.th

We have developed a portable neutron monitor ("Changvan") with three sections to investigate cosmic ray spectral variations via latitude surveys. The Changvan uses the NM64 design for two sections, but the third lacks the lead producer, so we call this a "semi-leaded" neutron monitor. The Changvan was operated on two voyages on the Chinese icebreaker *Xue Long* between Shanghai and Antarctica during 2019 and 2020. Repeated measurements with the same detector over different phases of the solar cycle provide precise information about cosmic ray spectral variation. In addition, we tested two techniques to track spectral variations, which can be implemented at fixed stations. The count rate ratio of unleaded vs. leaded counters varies with geomagnetic cutoff rigidity, indicating sensitivity to the cosmic ray spectrum. Histograms of the time delay between successive neutron counts determine the leader fraction, also used to monitor short-term and solar-cycle spectral variations. We report measurements of the response functions of the count rates and leader rates of the unleaded and leaded counters during these two latitude surveys.

37th International Cosmic Ray Conference (ICRC 2021)
July 12th – 23rd, 2021
Online – Berlin, Germany

*Presenter

PoS(ICRC2021)1251

1. Introduction

High-energy particles or "primary cosmic rays" originate from sources outside the solar system. In collisions between primary cosmic rays and nuclei in the Earth's atmosphere (such as nitrogen and oxygen) particles that we refer to as "secondary cosmic rays" are generated. The flux of primary cosmic rays varies with energy and the properties of the solar wind [1, 2]. In addition, the Earth's magnetic field excludes lower energy primary cosmic rays, so the flux depends on geomagnetic latitude. Many secondary cosmic rays are neutrons that can be detected by a neutron monitors (NM), which are ground-based cosmic ray detectors used to precisely track time variations in the Galactic cosmic ray flux energy ranges above the geomagnetic cutoff rigidity of a certain area. The standard NM64 design [3] comprises a neutron detector surrounded by a lead producer and polyethylene moderator and reflector. Without reflector and producer, we concisely call the isolated, moderated detector a "bare counter." In September 2018, we installed three BP-28 neutron detector tubes inside a standard shipping container – the so-called "Changvan" as shown in Figure 1. The center tube is nominally bare, but the polyethylene reflector still covers all three tubes as one unit. Thus the center tube is strongly influenced by the lead producer on the side tubes. We therefore refer to it as a "semi-leaded" neutron monitor (SLNM), since it has a higher count rate due to the adjoining lead. As such the SLNM/NM64 ratio will allow us to study spectral variations in a way related to the standard Bare/NM configuration but with a different response. The main purpose of the Changvan mobile monitor is – in the sense of the "Calmon [1]" – to tie together fixed neutron monitor stations measuring the "leader fraction [2, 4–6]." Latitude surveys are also useful in detecting short-time variations in the Galactic cosmic ray spectrum. By conveying the neutron monitor across a wide range of latitude, the Earth's magnetic field eliminates particles below a momentum per unit charge called rigidity at any given location. The geomagnetic cutoff can be accurately calculated using models of the geomagnetic field and limiting particle trajectory in the magnetic field. In this work, we report the measured response functions of the count rates and leader rates in 2019 and 2020 latitude surveys.

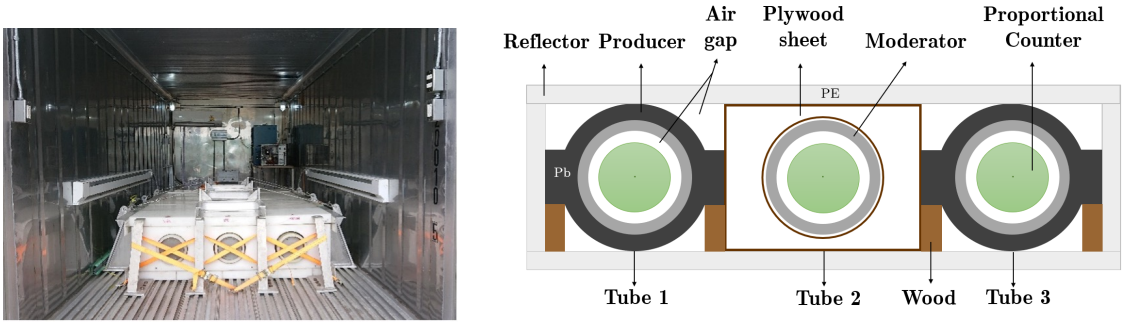

(a) (b)

Figure 1: (a) A photograph of the semi-leaded neutron monitor Changvan. (b) Drawing of the Changvan monitor. Tube 1 (left) and tube 3 (right) are NM64s. Tube 2 (middle) is an unleaded neutron monitor hold onto three supported wooden plates.

2. Observations

During the 2019 and 2020 survey years, the Changvan was carried by the icebreaker *Xue Long* on research missions conducted by the Polar Research Institute of China (PRIC). The "survey year" refers to the year in which the voyage ended. Survey year 2019 covers the voyage from 2 November 2018 to 11 March 2019, and survey year 2020 covers the voyage from 21 October 2019 to 22 April 2020. The 2019 survey year also called the 35th Chinese Antarctic Research Expedition (CN35) and the 2020 survey year is termed CN36. Because of the heavy load of other shipping containers on CN35 we were not able to operate the Changvan on the voyage from Shanghai to the Chinese research station in Antarctica, Zhongshan. We took data from Zhongshan back to Shanghai from 11 February 2019 to 11 March 2019. Figure 2 shows routes for the two survey years.

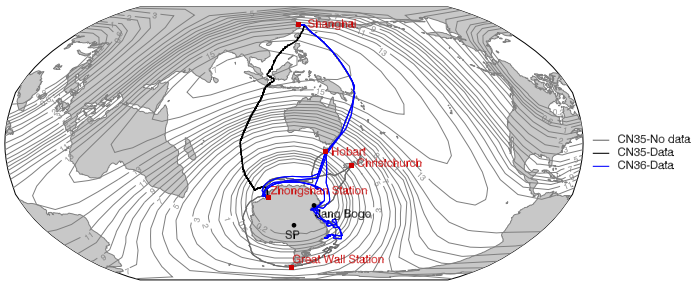

Figure 2: Tracks of the latitude surveys in 2019 and 2020, superimposed on contours of the vertical cutoff rigidity in GV, calculated for 11 February 2019 at 12:00 UT. In the survey year 2019 (CN35), the grey line shows the route of the Changvan without taking data, and the black line shows the route of continuous recording data of Changvan from Zhongshan station to Shanghai. In the survey year 2020 (CN36), the blue line shows the route of taking data from Shanghai to Zhongshan station and back.

3. Data

3.1 Data cleaning

The Changvan records one-second resolution count rate data and hourly time-delay histogram files. We demonstrate calculating the leader fraction from the time-delay histograms the next section. We did not clean up or applied any corrections, i.e., pressure, etc., to our histogram analysis in this work. But for the analysis of the count rate data obtained from the ship-borne neutron detectors, we cleaned data based on the one-second distribution and count rate ratios, and then corrected data for barometric pressure.

To correct the effects of changing configuration during the surveys, we used the inherent redundancy of the three detectors. We have several steps to clean the data appropriately. In the first step, we considered the recorded counts for each second. We then made histograms of the 1-second distribution for each tube for each hour. We removed three types of bad seconds from an hour, as reported in [8]. The first type of bad data is obvious outliers that accumulate ≥ 30 counts in one second. The second type we call "frozen data" with the same count for all three tubes for at least three consecutive seconds. The last type is a second in which all tubes record zero counts. After cleaning counts based on the 1-second distribution discussed above, we estimated each tube's hourly

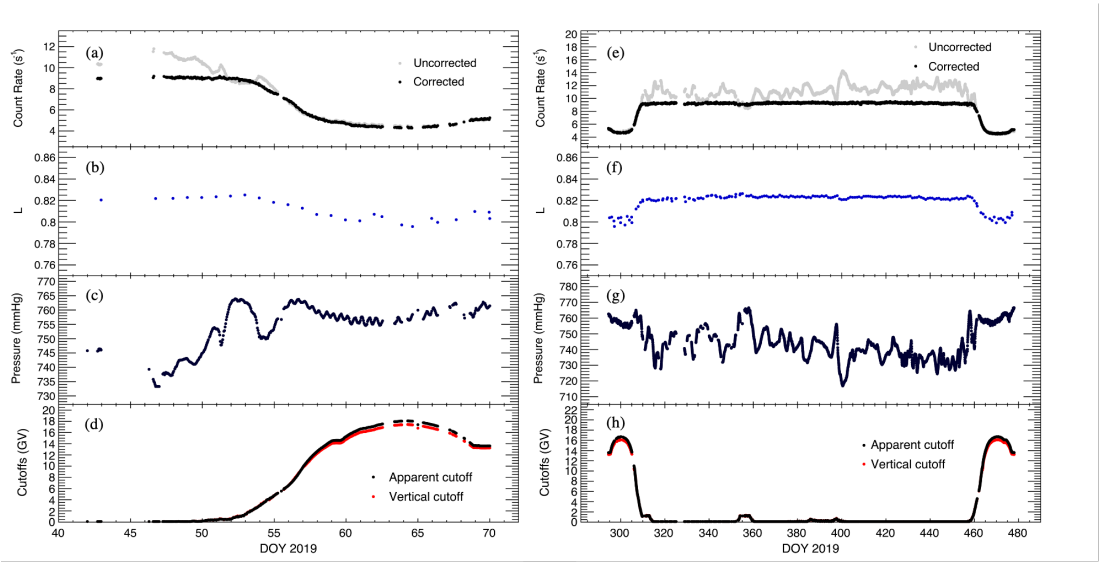

Figure 3: (a)-(d) Data set of the survey year 2019 and (e)- (h) of the survey year 2020, as a function of time. (a) and (e) Hourly averaged count rates for two counter tubes (T1 & T3). (b) and (f) display daily uncorrected L for pressure. More detail of calculating L is explained in the text. (c) and (g) The barometric pressure was recorded by GPS on the *Xue Long* icebreaker. (d) and (h) show geomagnetic cutoff rigidity, where the black line shows the apparent cutoff rigidity, and the red line shows the vertical cutoff rigidity [9–11].

average count rate. The middle lead-free neutron counter (T2) in between the left (T1) and the right (T3) is very sensitive to environments and surroundings. We used a higher level of deviation for the ratios regarding T2 for greater statistical accuracy. We removed points outside a range of three standard deviations ($\pm 3\sigma$) for T3/T1 count rate ratio, four standard deviations ($\pm 4\sigma$) the T1/T2 and T2/T3 count rate ratios, all relative to the mean value of the Gaussian distribution [8].

During 21-24 November 2019 (CN36), other shipping containers were loaded on top of the Changvan container when the ship docked at Zhongshan station in Antarctica. We noticed that the count rate decrease significantly, so we decided to remove the data during that time because we did not want the data to be contaminated. After November 24, the count rates for all three tubes markedly increased throughout the voyage back to Shanghai. It is hard to interpret how things are placed around the Changvan shipping container. Luckily, the ship detoured nearby Jang Bogo Station (JBGO) in Antarctica, a South Korean research station, a few times; see blue line in Figure 2. This allows us to calibrate northbound ship-borne data for each tube from the ratios of mobile vs. JBGO pressure-corrected count rates downloaded from https://www.nmdb.eu/. We obtained the normalization factors throughout the way back after 24 November 2019 for T1, T2, and T3 are 1.1167, 1.0949, and 1.0687, respectively. The data calibrated with JBGO, but uncorrected for pressure is shown in gray of Figure 3(f).

3.2 Barometric pressure correction

We collected data with the same system used in previous surveys [7] as shown in Figure 3. The count rate of each counter was recorded together with the attitude of the ship (pitch and roll). The barometric pressure also was recorded, as was the position of the ship derived from GPS data.

JBGO has been used to estimate solar modulation changes and calibrate data in the survey year 2020 (CN36). Geomagnetic cutoff rigidity [9–11] was calculated at one hour intervals.

In Figure 3, we can see that the count rate has the expected strong anticorrelation with barometric pressure. A major correction for variation in barometric pressure is necessary to estimate the response functions properly. Here, we used Eq. (3) of [7] derived from 13 surveys with substantially equivalent instruments to calculate the pressure coefficient β in units of percent per mmHg changing with cutoff rigidity. We corrected the observed count rate to sea level, the atmospheric pressure of 760 mmHg, to remove fluctuations in the data.

4. Analysis of neutron time-delay histograms

Time-delay histograms manifest the relation between the distribution of the count rate of successive secondary cosmic rays (particularly neutrons) and time intervals of the neutron counter tube. By using time delay histograms from a neutron monitor can accurately track time variations in the flux of Galactic cosmic rays (GCRs). We analyze hourly time-delay histograms collected by Changvan neutron monitor during the 2019 and 2020 survey years to calculate the leader fraction (L) [6]. The data acquisition system produces time delay histograms for each counter over short and long timescales. For the short time delay histograms, the system records the frequency of time delays in 1024 time bins of width t_s = 0.0021701 ms, so the time width frame is approximately 2.222 ms. The long time delay histograms contains 1024 bins of nominal width t_l= 64×t_s = 0.1389 ms. The last time bin at (t_o= $2^{16} \times t_s$ = 1024 × 0.0021701 = 0.142 s contains time delay overflows. We examined L throughout the 2019 and 2020 surveys, shown in Figure 3(b) and Figure 3(g). An example analysis of long and shot time delay histogram in one hour has been shown in Figure 4(left) and 4(right) respectively. The green vertical line in Figure 4(right) shows the electronics dead time (t_d) for each tube, which about 87 μs (following the methods of [4]). The short time delay histogram for T1 and T3 display sharp peaks as the neutrons from the producer can reach the detector directly and rapidly. For the unleaded monitor (T2) in Figure 4(right), the rapid peak is much smaller because the neutrons must propagate from the producers from both sides. Figure 4(left), shows the long time delay distribution for one hour from the three counter tubes, Leader fraction (L) determination is the technique for analyzing time-delay histograms to remove the effect of chance coincidences of neutrons that did not follow a prior neutron count in the same counter tube due to the same atmospheric secondary particle [4]. Fitted $N(t)$, $A_o e^{-\alpha t}$, from 5 ms to before the last time bin (excluding the overflow time bin) [6] is shown in red. The amplitude of exponential tail gives the rate of "leaders" arriving by chance, not "following" in temporal association with preceding count. The A_0 and α parameters are used to calculate L [5]. In this work, we applied the dead time t_d in our analysis, and normalized each long time delay histogram to account for missing values at t > t_o:

$$L = \frac{\int_{t_d}^{\infty} A_o e^{-\alpha t} dt}{\int_{t_d}^{t_o} N(t) dt + \int_{t_o}^{\infty} A_o e^{-\alpha t} dt} \tag{1}$$

for the discrete histogram,

$$L = \frac{\frac{A_o}{\alpha} e^{-\alpha t_d}}{\sum_{t=t_d}^{t_o} N_t + \frac{A_o}{\alpha} e^{-\alpha t_o}} \tag{2}$$

where α and A_o are the parameters from the hourly long-time histogram fit. As being said, t_o= 0.142 s is the overflow time in the electronic system, and dead time t_d = 87 μs [2, 5]. The term $\sum_{t=t_d}^{t_o} N_t$ is the sum of neutron pulses for all time bins from t_d to t_o from the recorded histogram.

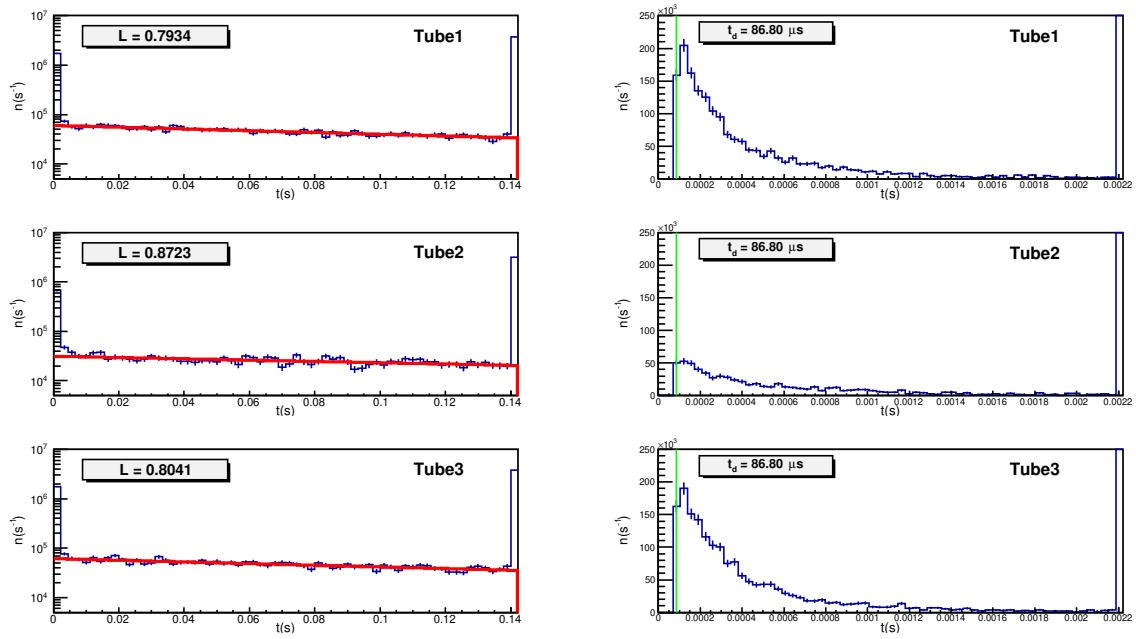

Figure 4: Analysis of time delay histogram for each counter tube for one hour. Here is an example of the 15$^{\text{th}}$ hour UT on the 3$^{\text{rd}}$ September 2019. (left) Analysis of long time delay histogram, and (right) analysis of short time delay histogram, the green vertical line shows the electronics dead time (t_d), which is about 87 μs.

5. Response functions

We used the averaged data between T1 and T3 to find the response functions of the Changvan neutron monitor because T2 has a different configuration. We multiplied leader fraction (L) values to the count rate (N) for each cutoff rigidity bin, i.e., 0-1 GV, 1-2 GV,..., 17-18 GV, allowing us to derive what we called "leader rate (R)." The R supersedes the count rate that removed a chance of coincidence from the same secondary cosmic ray particles in the neutron monitor to avoid problems with multiplicity in a fixed time window. Multiplicity is expected to be dominated by the composition of secondary atmospheric particles and their energy.

Figure 5 presents two types of analysis of the survey data: the classic approach of determining count rate response function, and analysis of leader rate response function. At this stage, we have N and R corresponding to apparent cutoff rigidity (P_c). The results are fitted to a commonly used parameterized function of P_c, the "Dorman function" [12]. Even though the Dorman parameterization has no physical meaning, it provides a great representation of the integral response function for count rate (N) and leader rate (R). Our fits to determine Dorman parameters excluded data from rigidities below 0.15 GV and excluded all data hours the ship was not moving at the ports.

Table 1: Derived Dorman Parameters for count rates and leader rates for 2019 and 2020 survey years

Survey Year	Name Tag	Analysis	N_0	α	κ	R_0	α'	κ'
2019	CN35	(T1+T3)/2	8.865	6.843	0.8069	7.320	6.434	0.7999
2020	CN36	(T1+T3)/2	8.958	8.539	0.8810	7.363	8.140	0.8769
2020	CN36	T2	5.837	8.058	0.8380	5.249	7.611	0.8317

$$N(P_c) = N_0(1 - e^{-\alpha P_c^{-\kappa}}) \text{ and } R(P_c) = R_0(1 - e^{-\alpha' P_c^{-\kappa'}}). \quad (3)$$

The DRF is defined as the integrand of the integral count rate response function, and the DLF is defined as the integrand of the integral leader rate response function:

$$N(P_c) = \int_{P_c}^{\infty} DRF(P)dP \text{ and } R(P_c) = \int_{P_c}^{\infty} DLF(P)dP, \quad (4)$$

$N(P_c)$ and $R(P_c)$ can be differentiated to determine the DRF and DLF, respectively.

$$DRF(P) = N_0\alpha\kappa P^{-\kappa-1}e^{-\alpha P^{-\kappa}} \text{ and } DLF(P) = R_0\alpha'\kappa' P^{-\kappa'-1}e^{-\alpha' P^{-\kappa'}}, \quad (5)$$

where N_0, α, and κ are fitted parameters for count rate and R_0, α', and κ' are fitted parameters for leader rate. The values of these six "Dorman paramters" for 2019 and 2020 survey years from analysis corresponding to Figure 5 of our pressured corrected data are shown in Table 1.

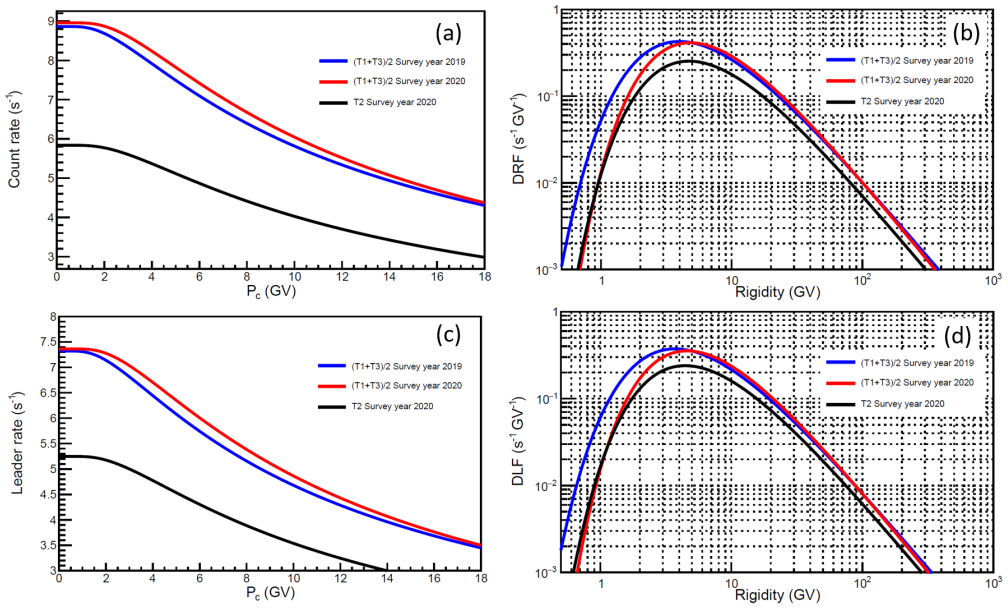

Figure 5: Dorman function fits Vs. P_c for 2019 and 2020 survey years. (a)-(b) Integral and differential count rate response functions. (c)-(d) Integral and differential leader rate response functions.

6. Conclusions

We have analyzed data and determined the response functions as a function of apparent cutoff rigidity of the count rates and leader rates of the unleaded (T2) and leaded counters (averaged T1

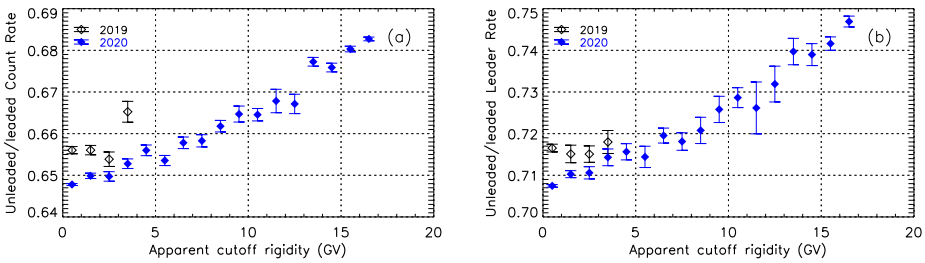

Figure 6: The count rate (left) and leader rate (right) ratio of unleaded vs. leaded counters as a function of apparent cutoff rigidity for the 2019 and 2020 survey years. Here, "unleaded" means T2, and "leaded" means the averaged T1 and T3. Error bars indicate the standard error.

& T3) of 2019 and 2020 latitude surveys. In Figure 6, we can see the count rate and leader rate ratio of unleaded vs. leaded counters varies linear trend with geomagnetic cutoff rigidity, indicating sensitivity to the cosmic ray spectrum.

7. Acknowledgments

The research is supported in part by Thailand Science Research and Innovation via Research Team Promotion Grant RTA6280002. We thank the Northern Science Park (Chiang Mai) for providing laboratory space at the park, which helps the research team working smoothly.

References

[1] Aiemsa-ad, N. et al. (1964), J. Geophys. Res. Space Phys., 120, 21249

[2] Mangeard, P.-S., D. Ruffolo et al. (2016), J. Geophys. Res. Space Phys., 121, 11,620–11,636

[3] Hatton, C. J. & H. Carmichael (1964), Can. J. Phys., 42, 2443–2472

[4] Ruffolo, D., et al. (2016), Astrophys. J., 817, 38

[5] Banglieng, C., et al. (2020), Astrophys. J., 890, 21

[6] Yakum, P., et al. (2021), J. Phys.: Conf. Ser., 1719

[7] Nuntiyakul, W., et al. (2014), Astrophys. J.,795, 11

[8] Khamphakdee, S., et al. (2021), J. Phys.: Conf. Ser., 1719

[9] Bieber, J., J. Clem, P. Evenson et al. (1997), In Proc. of the 25th ICRC, 2, 389–392

[10] Clem, J., J. Bieber, P. Evenson et al. (1997), J. Geophys. Res., 102, 26,919–26,929

[11] Lin, Z., J. Bieber & P. Evenson (1995), J. Geophys. Res., 100, 23,543–23,550

[12] Dorman, L. I. et al. (1970), In Proc. of the 11th ICRC, 2, 233